Schweizerische Eidgenossenschaft
Confédération suisse
Confederazione Svizzera
Confederaziun svizra

Federal Department of the Environment, Transport, Energy and Communications DETEC

**Swiss Federal Office of Energy SFOE**
Energy Research and Cleantech Division

**Final report dated** 07 March 2023

# Thermal heat storage in fractured reservoirs

## Geothermal energy storage systems

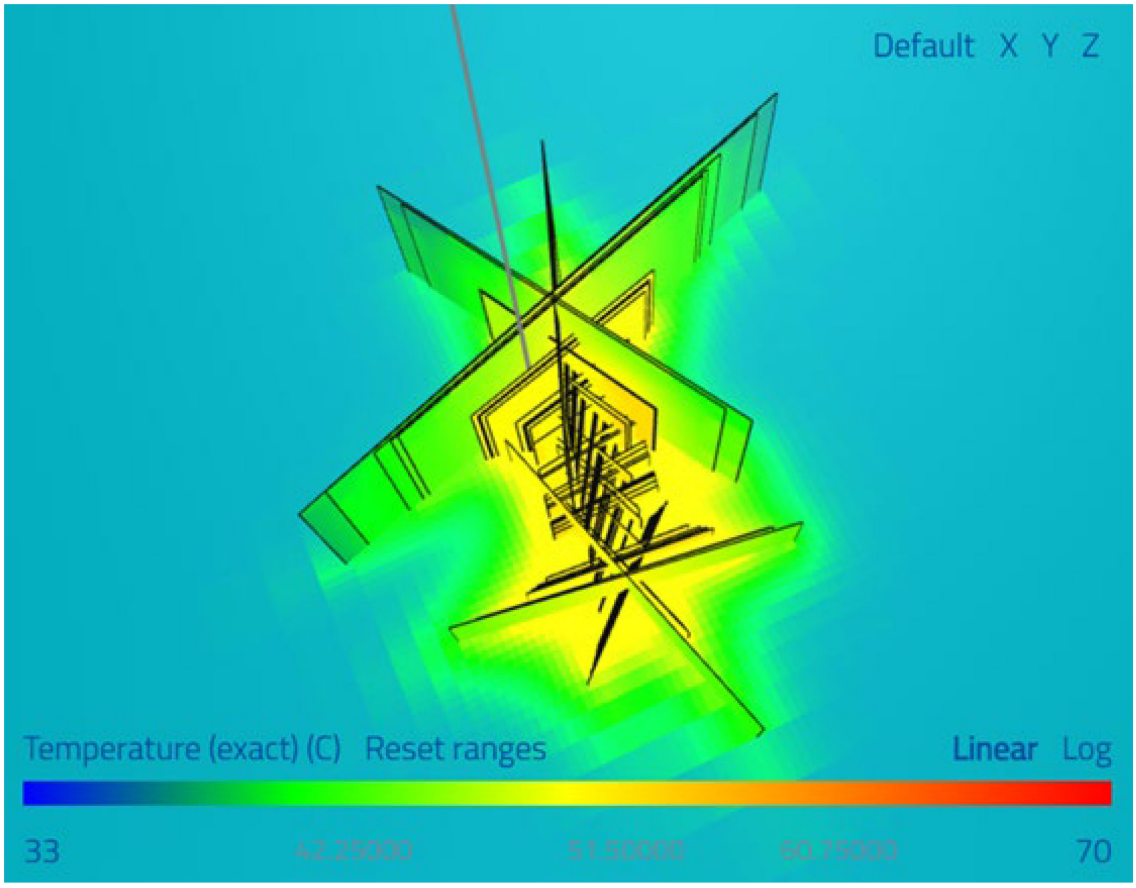

**Date:** 07 March 2023

**Location:** Bern

**Publisher:**
Swiss Federal Office of Energy SFOE
Energy Research and Cleantech
CH-3003 Bern
www.bfe.admin.ch

**Authors:**
Janz, Rondon, ResFrac Corporation, janz@resfrac.com
Mark, McClure, ResFrac Corporation, mark@resfrac.com

**SFOE project coordinators:**
Valentin Gischig, valentin.gischig@bfe.admin.ch
Stefano Benato, stefano.benato@bfe.admin.ch

**SFOE contract number:** SI/502482-FTES ResFrac

# Summary

Energy storage is a critical component of a low carbon energy infrastructure. For example, heat may not be needed at the time of generation (e.g. in summer), but if efficiently stored, it could be useful in times of high heat demand (e.g. in winter).

This project evaluates two geothermal energy storage systems based on geologic/thermal properties of a typical fractured reservoir in crystalline rock. Using a fully-coupled fracturing, wellbore, and reservoir numerical model, two scenarios were evaluated: one for thermal storage within a single, fracture-stimulated well, and the other for thermal storage in a well pair (connected with fractures with stimulated injectivity). The systems are operated in seasonal injection/production cycles, injecting waste heat in the summer when not needed, and producing warm fluid back in the winter.

The conductivity of the fractures was calibrated to have similar stimulated injectivity as observed in fractured crystalline basement, such as at the Bedretto Underground Laboratory in Switzerland. The dominant operational parameters such injection and rate, injection temperature, and bottomhole pressure were adjusted to obtain an efficient energy storage system. The results were evaluated based on power and energy input, power and energy output, and overall efficiency. A sensitivity analysis was performed on the well pair model to understand the impact from well spacing.

# Main findings

In practice, the formation injectivity/productivity will be a critical determining factor for performance. If the system permeability is too low, it will not be possible to achieve sufficient injection and production rates. However, considering parameters inspired by the Bedretto Underground Laboratory in Switzerland, it appears that such injectivities can be achievable, especially if wells utilize extended open-hole sections. Borehole orientation (vertical, deviated, or horizontal) should be optimized to maximize the number of natural fractures that are intersected, considering the dominant fracture network orientations. Hydraulic stimulation may be a useful tool to increase injectivity/productivity.

# 1 Introduction

## 1.1 Background information and current situation

In many countries - incl. Switzerland - heating demand peaks during the winter months. A variety of Underground Thermal Energy Storage (UTES) systems exist to allow seasonal storage of waste and/or low-carbon renewable heat sources during the summer months, which can be extracted during the winter months to help cover heating demand. Several Swiss energy, industry, utility, and waste-to-energy operators are interested in storage and recovery of thermal energy in the subsurface (i.e., SIG, EWB, Nestlé, etc.).

Underground Thermal Energy Storage (UTES) includes: Aquifer (ATES), Borehole (BTES), Tank (TTES), Pit (PTES), Cavern (CTES), and Fractured (FTES) thermal energy storage methods (Hellström and Larson 2001, Pavlov and Olesen 2012, Novo et al. 2010).

The most desirable storage media for sensible heat storage should: 1) provide a substantial change in internal energy per unit volume, 2) be mechanically stable, 3) have low toxicity and corrosiveness, and 4) be inexpensive (Barnes and Levine 2011, Cabeza 2015, Janiszewski 2019). With this in mind, crystalline hard rocks and water are both considered to be good storage media, due to their favorable properties and ability to obtain large storage volumes at relatively low costs (Nordell and Hellström 2000, Janiszewski 2019). Crystalline rocks - consisting primarily of granites and gneisses - are widely found in the Central and Southern Swiss Alps.

Fractured thermal energy storage (FTES) systems involve the use of natural or artificially induced fractures in low-permeability crystalline rocks for storage and extraction of thermal energy. This type of open-loop storage system consists of multiple, interconnected fracture networks intersected by a number of boreholes (Janiszewski 2019).

## 1.2 Purpose of the project

This study investigates the feasibility of using geothermal injection/production for storage of waste heat from summer months so that it can be used in the winter months. Two scenarios are considered in a series of numerical models: (a) a single well with injection during the summer and production during the winter, and (b) a doublet where Well 1 is used for injection during the summer and production during the winter, the Well 2 is used for injection during the winter and production during the summer.

In practice, the performance of these systems will depend on site-specific reservoir characteristics. This study is a generic, high-level assessment of overall feasibility, and not an analysis of a particular reservoir. As a baseline, the reservoir properties are chosen to be similar to those of Bedretto Underground Laboratory for Geosciences and Geoenergies (Gischig et al. 2020).

# 2 Procedures and methodology

## 2.1 Modeling approach

The numerical simulations were performed with ResFrac, an integrated hydraulic fracturing, reservoir, and wellbore simulator (McClure et al. 2022). The simulations employ a 'discrete fracture network' embedded in a relatively impermeable matrix.

## 2.2 Base model construction and parameterization

The formation properties for the base model lean on the properties of the Bedretto Reservoir Project (BRP) (Bröker 2019, Ma et al. 2021, Birdsell et al. 2021, Giardini et al. 2022, Bröker et al. 2022) All the simulation scenarios use the same base model, which represents a fractured crystalline formation at 1000 m depth (comparable to that of the Bedretto Lab). In some cases, literature review was used to select 'reasonable' values for input parameters (David et al. 2020, Cho et al. 2010).

Table 1 provides the geomechanical properties, and Table 2 provide thermal and reservoir properties.

Table 1: Geomechanical properties (1000 m target depth)

| Property | Literature range (metric) | Model (metric) | Model (oilfield) |
|---|---|---|---|
| Shmax azimuth | 100˚ - 110˚ | 105˚ | 105˚ |
| Frac gradient | 12.0 – 14.4 MPa/km | 13.6 MPa/km | 0.60 psi/ft |
| Frac toughness | 1.32 MPa m^(1/2) | 1.32 MPa m^(1/2) | 1200 psi in^(1/2) |
| Rock density | 2590 - 2630 kg/m^3 | 2610 kg/m^3 | 163 lb/ft^3 |
| Overburden gradient | | 25 MPa/km | 1.11 psi/ft |
| Pore pressure gradient | 2.2 – 5.0 MPa/km | 5.0 MPa/km | 0.23 psi/ft |
| Poisson ratio | 0.33 - 0.40 | 0.36 | 0.36 |
| Youngs modulus | 38 – 54 GPa | 44 GPa | 6.7e6 psi |
| Biots coefficient | | 0.5 | 0.5 |

Table 2: Thermal and petrophysical properties (1000 m target depth)

| Property | Literature range (metric) | Model set up (metric) | Model set up (oilfield) |
|---|---|---|---|
| Porosity | 1.2% – 1.7% | 1.4% | 1.4% |
| Permeability | 1.1e-18 - 1.4e-18 m^2 | 1.25e-18 m^2 | 0.00125 µd |
| Surface temperature | | 12˚C | 54˚F |
| Temperature gradient | 20 – 30˚C/km | 25˚C/km | 4.5˚F/(100ft) |
| Temperature at 1000 m depth | | 37˚C | 77˚F |
| Rock heat capacity | 800 – 850 J/(kg-K) | 816 J/(kg-K) | 0.195 BTU/(lb-R) |
| Thermal conductivity | 3.17 – 3.44 W/(m-K) | 3.3 W/(m-K) | 1.91 BTU/(hr-ft-F) |

## 2.3 Single and double wellbore configurations

This study evaluates two different well configurations:

1. A single well configuration with injection during the summer season and production during the winter season.

2. A double well model in which Well 1 is used for injection during the summer and production during the winter, and Well 2 is used for injection during the winter and production during the summer.

Both models assume wellbore ID (interior diameter) of 0.097 m . The vertical section has a casing with an estimated heat transfer capacity of 51 [W/(m^2-K)] and the horizontal section is openhole.

## Single well model

The wellbore has a 1000 m vertical section, and then it is deviated into a 100 m horizontal section. Note that this differs from the Bedretto borehole setup, in which inclined boreholes are drilled from a cavern at 1000 m depth.

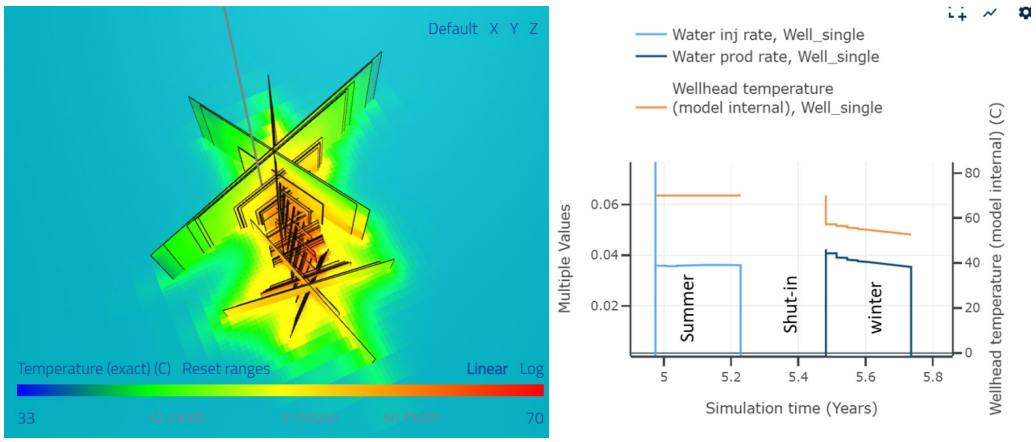


Figure 1: Screenshot showing the single well configuration.

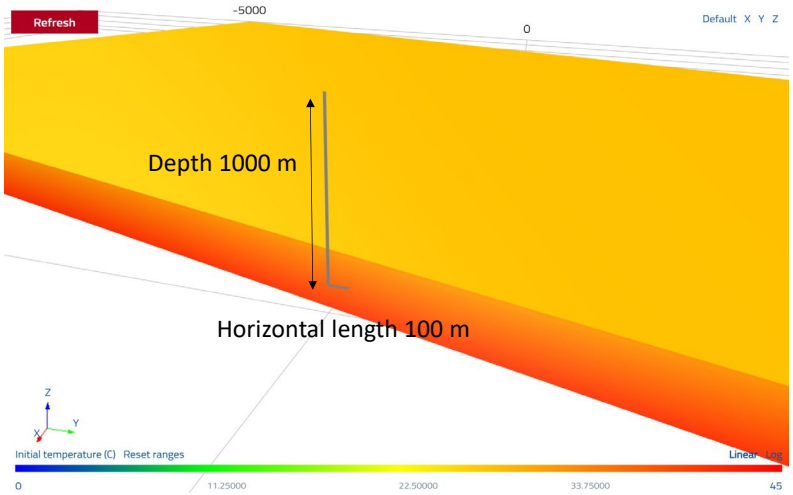


Figure 2: Screenshot showing the single well configuration.

## Double well model

In the double well configuration, both wells have a 1000 m vertical section and a 100 m horizontal section. They are laterally separated by 50 m.

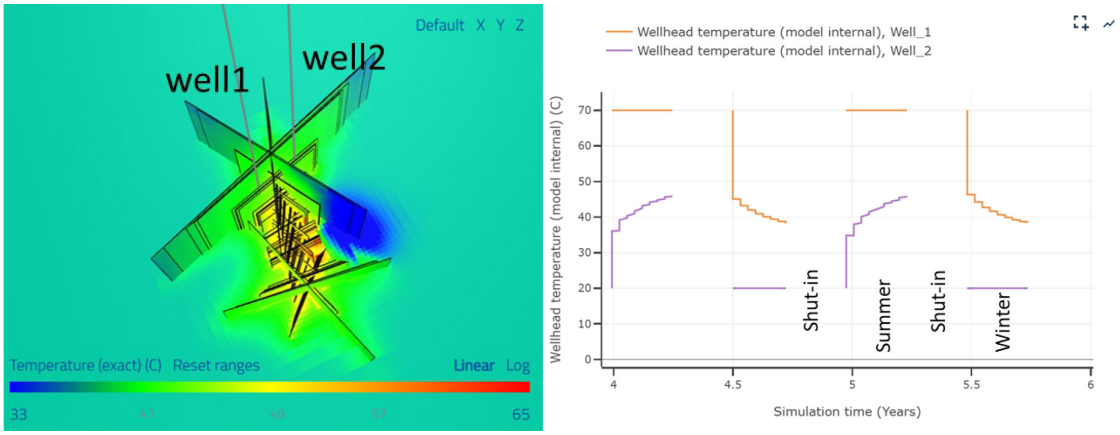


Figure 3: Screenshot showing the two well configuration.

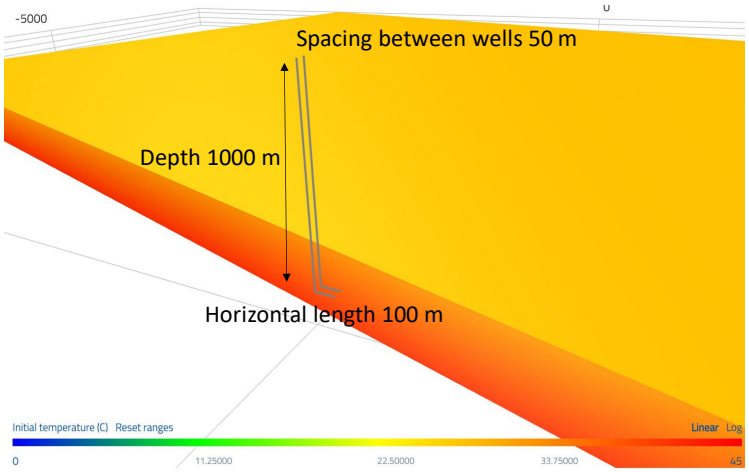


Figure 4: Screenshot showing the two well configuration.

## 2.4 Confirming numerical accuracy

Early in the construction of the base mode, we compared the results from two meshing methods: (a) a relatively coarse ‘global’ mesh with the 1D submesh method for calculating flow and heat conduction between fractures and the matrix elements (McClure 2017), and (b) a conventional approach with a highly refined mesh.

A simple test problem was set up with a single preexisting fracture. Two cycles of injection and production were performed. The simulation results were similar between the two approaches.

The 1D submesh approach is much more computationally efficient, and so we decided to use the 1D submesh approach in subsequent simulations.

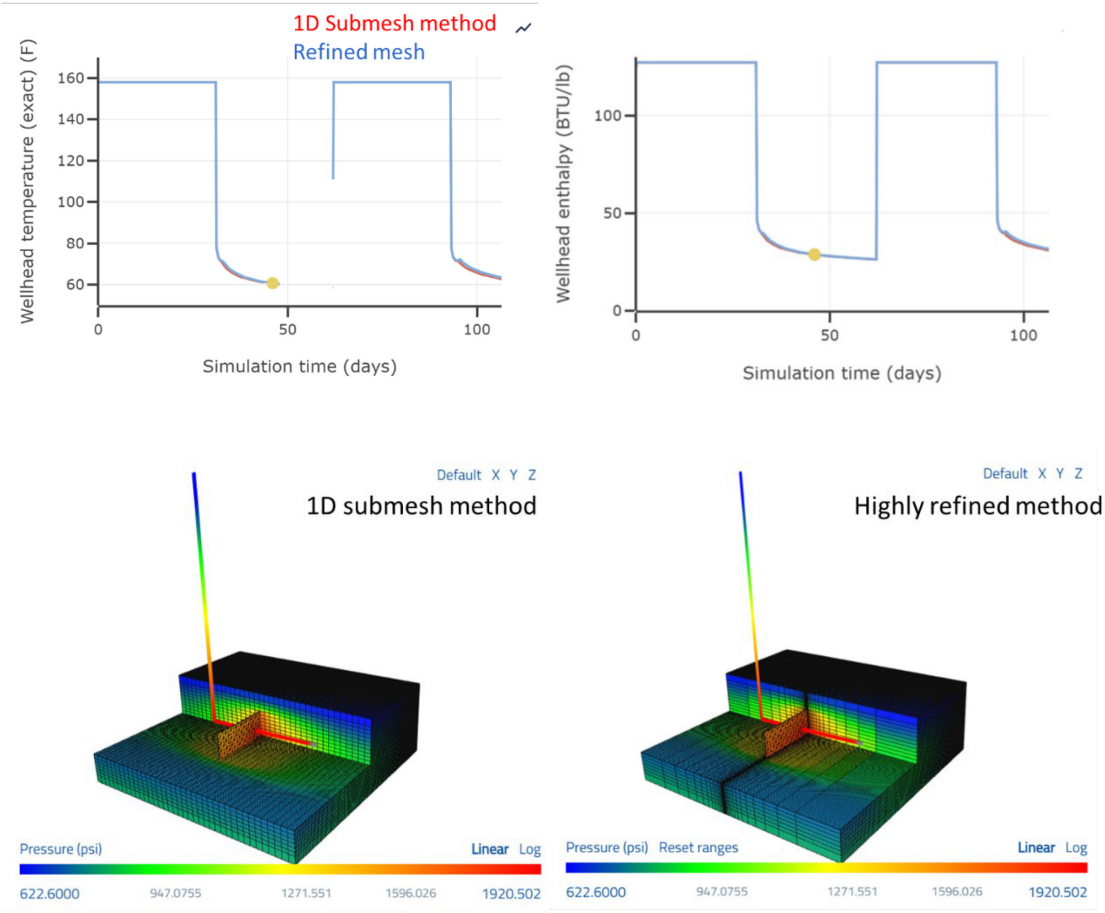


Figure 5: Injection and production temperature and enthalpy, and the 3D distribution of fluid pressure, for a simple test problem with a single fracture.

## 2.5 Simulation domain considerations

The simulation domain was made very large in order to avoid boundary effects. The mesh is a square with 14 km length. To avoid excessive number of elements, the mesh uses a smaller element size in the near-field (closer to the wellbore), with increasing mesh size further from the wellbore.

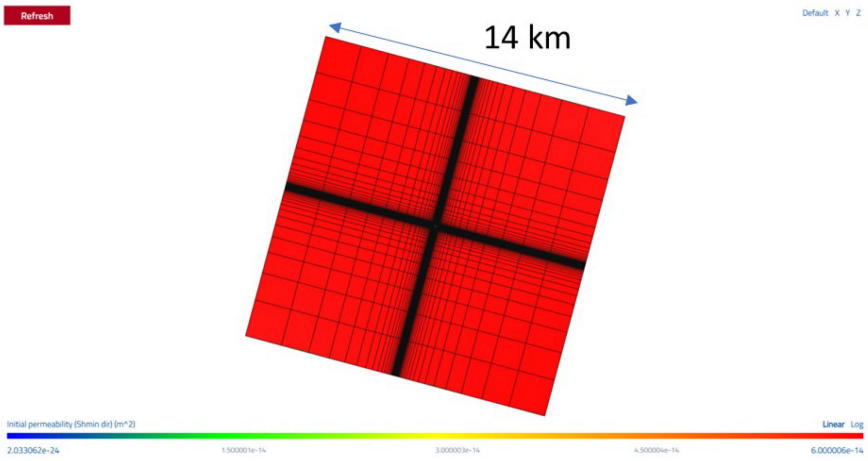


Figure 6: Aerial view of the simulation mesh.

A discrete fracture network approach was used to simulate the heat and mass transfer effects particular to flow in fractured rock. However, it is not computationally feasible to create a DFN that fills the entire 14x14 km reservoir domain. To address this problem, a DFN was used in the region immediately surrounding the wells, and an ‘effective continuum’ approximation was used outside this region. As shown below, the matrix permeability was made higher in the ‘effective continuum’ region, in order to account for the ability of the fractures to accommodate flow, which increases the ‘system permeability’ above that of the intact matrix.

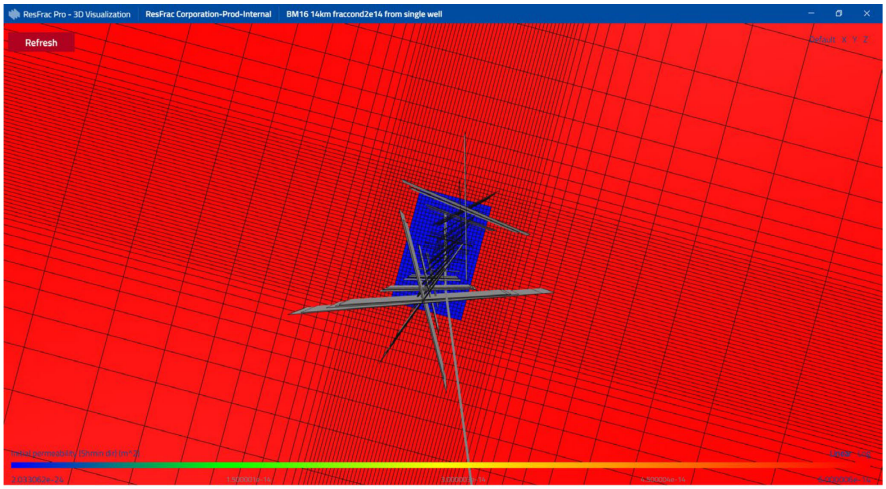


Figure 7: Aerial view showing the DFN region and the surrounding ‘effective continuum’ region with elevated ‘effective’ permeability.

## 2.6 Discrete fracture network (DFN)

We considered three main fracture families in our model domain (similar to the crystalline reservoir in the Bedretto Underground Laboratory):

- Group 1 - NE-SW ~ 50 degree azimuth +/- 15
- Group 2 - E-W ~ 100 degree azimuth +/-15

- Group 3 - N-S ~ 0 degree azimuth +/-15

The first two groups are likely to be more predominant. For more details on the Bedretto fracture network observations, refer to Figure 7 from Ma et al. (2022).

The model in this study includes a discrete fracture network (DFN) with 131 fractures, and with orientations based on these three groups. The discrete fracture network has the distribution of fracture lengths and heights shown in Figure 8. The minimum length is 61 m and maximum length of 323 m, with an average length of 89 m. The minimum height is 41 m and maximum height of 122 m, with an average height of 57 m. The average aspect ratio of the fractures is 0.66 (height/length).

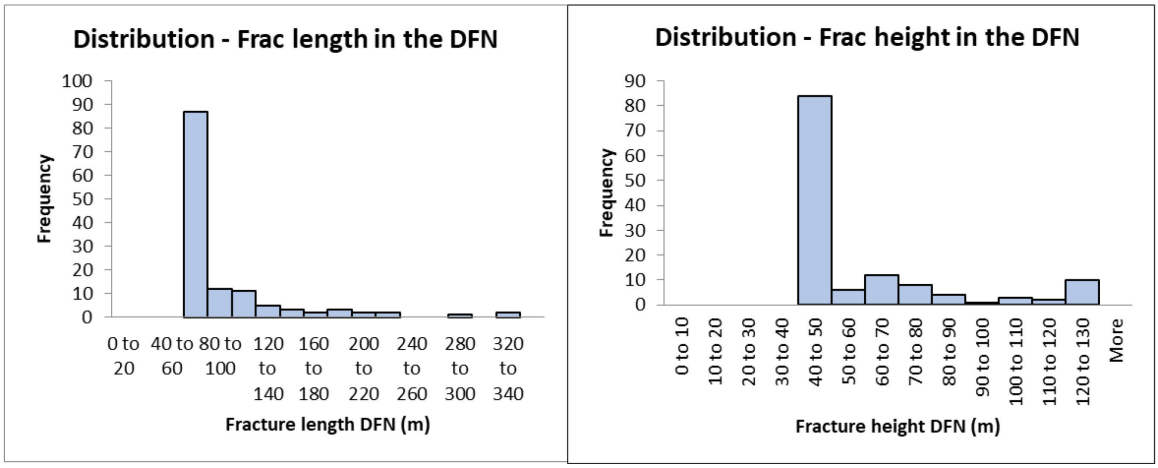


Figure 8: Distribution of the fracture length and heights in the DFN.

Table 3 provides orientation and size statistics for the DFN used in the simulations.

Table 3: Orientation and size statistics for the DFN used in this study.

| | Distribution | Number fracs |
|---|---|---|
| **Group 1 DFN NE-SW ~ 50 azimuth** | 60% | 78 |
| **Group 2 DFN E-W ~ 100 azimuth** | 30% | 39 |
| **Group 3 DFN N-S ~ 0 azimuth** | 10% | 13 |

| | Length (m) | Height (m) | Orientation |
|---|---|---|---|
| **min** | 61 | 41 | 35 |
| **max** | 323 | 122 | 179 |
| **average** | 89 | 57 | 76 |

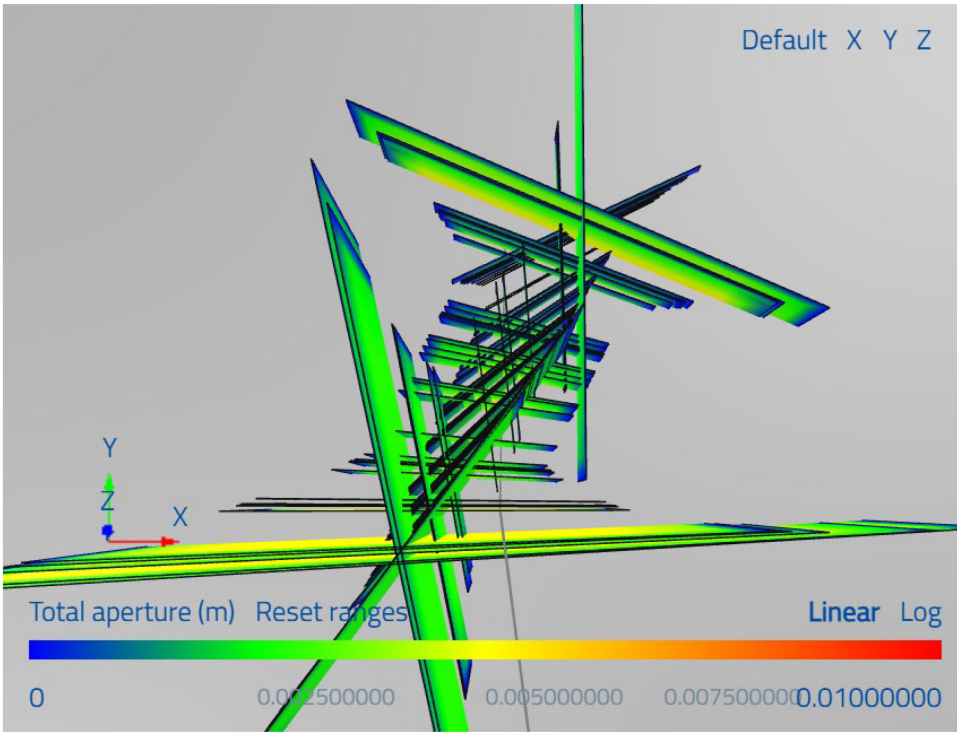


Figure 9: Screenshot showing the DFN used in the simulations.

# 3 Results and discussion

## 3.1 Calibration to the observed Injectivity index per length

First, the fracture conductivity was calibrated to match the observed average post-stimulation injectivity at the Bedretto Lab, 6 L/min/(MPa-m) using the injection rates observed post-stimulation as part of the VALTER sub-project (Giardini et al. 2022).

The results from the injectivity test post-stimulation on borehole ST1 (Giardini et al. 2022) were used to calculate the injectivity index that was used in the model. The average post-stimulation injective index was calculated as 6.3 (L/min)/(Mpa*m) as shown in Table 4.

Table 4: Calculated injectivity index using the results from post-stimulation in borehole ST1 (Giardini et al. 2022).

| Well | Interval | Post-stim Rate (L/min)/[4MPa] | Interval length (m) | Post-stim Rate (L/min)/[deltaP(MPa)* interval length(m)] |
|---|---|---|---|---|
| ST1 | 6 | 110 | 52 | 2.1 |
| ST1 | 4 | 335 | 8 | 41.9 |
| ST1 | 1 to 2 | 149 | 34 | 4.4 |
| **Total** | | **594** | **94** | **6.3** |

The model was calibrated to match the observed post-stimulation injectivity index using the equation:

$$Injectivity\ index\ per\ length = \frac{Injection\ rate\ rate}{(BHP - initial\ pore\ pressure) * (Openhole\ length)}$$

The calibrated model has an injection rate 0.03 $m^3/s$ with BHP 13 MPa after two days, corresponding to an injectivity of 6.1 (L/min)/(MPa*m), matching the observed injectivity, 6.3 (L/min)/(MPa*m) (Giardini et al. 2022). The calibrated fracture conductivity in the discrete fracture network (DFN) is 3e-14 m^3.

In all simulations, injection pressure is kept below the magnitude of Shmin to prevent the re-opening of the fractures during the injection period.

A special 'without DFN' simulation was run to calibrate the effective permeability used in the 'non-DFN' section of the model. The resulting system permeability estimate was 9e-14 m^2.

## 3.2 Single well model results

In the single well configuration, injection is performed for 3 months in the summer, and production is performed for 3 months in the winter. The injection and production rates are in the range of 0.03 to 0.04 m^3/s. The simulation is performed for six total years.

Injection is performed at a maximum BHP of 13 MPa (Figure 10), i.e. 3 MPa above hydrostatic pressure. Note that it is well possible that hydro-shearing (but not hydrofracturing) may occur at these levels of overpressure. Production is performed at a minimum BHP of 7 MPa. This sub-hydrostatic BHP would only be possible with the use of a production pump. Without a pump to produce at BHP below reservoir pressure, we found that it was not possible to maintain a balance between injection volume in the summer and production volume in the winter.

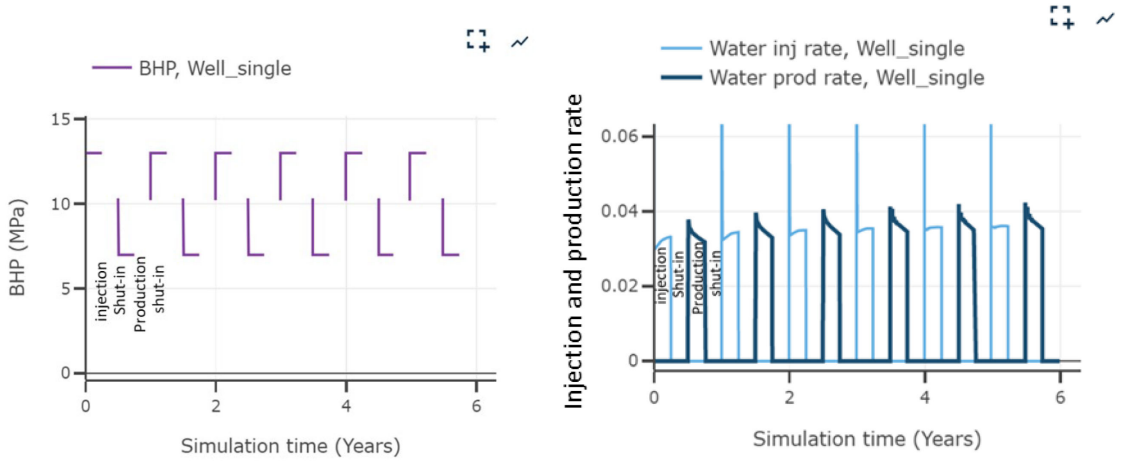


Figure 10: Results from the single well model showing the bottomhole pressure, injection and production rates.

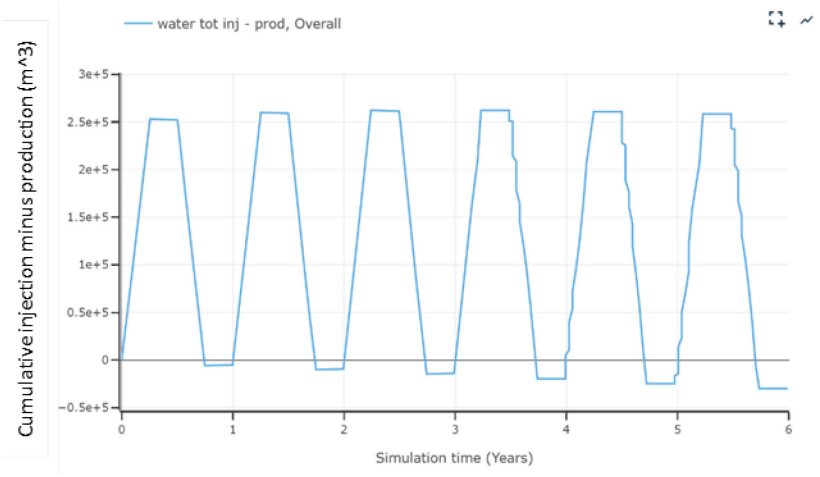


Figure 11: Results from the single well model showing cumulative water injection minus water production during the six one-year cycles.

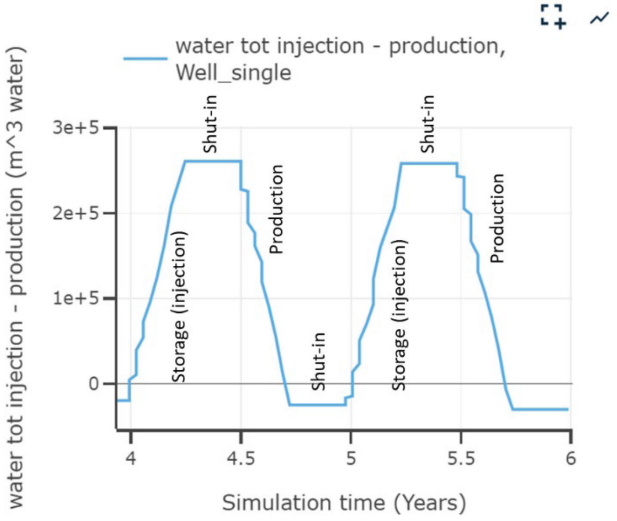


Figure 12: Results from the single well model showing cumulative water injection minus water production during the final two cycles.

Note that significant volumes of water are injected into the reservoir in this single-hole configuration (ca. 250’000 m3).

The model assumes the use of waste heat and the injection temperature in the summer is set at 70˚C. When fluid is produced back in the winter, the simulated produced fluid temperature is in the range of 44-49˚C during the first year, and 53-58˚C by the sixth year. There is a general trend that the production temperature increases from year-to-year.

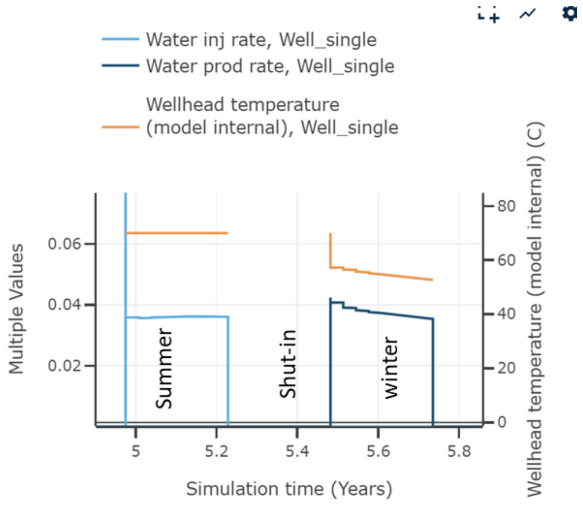


Figure 13: Results from the single well model with the injection and production temperatures during the final one-year cycle.

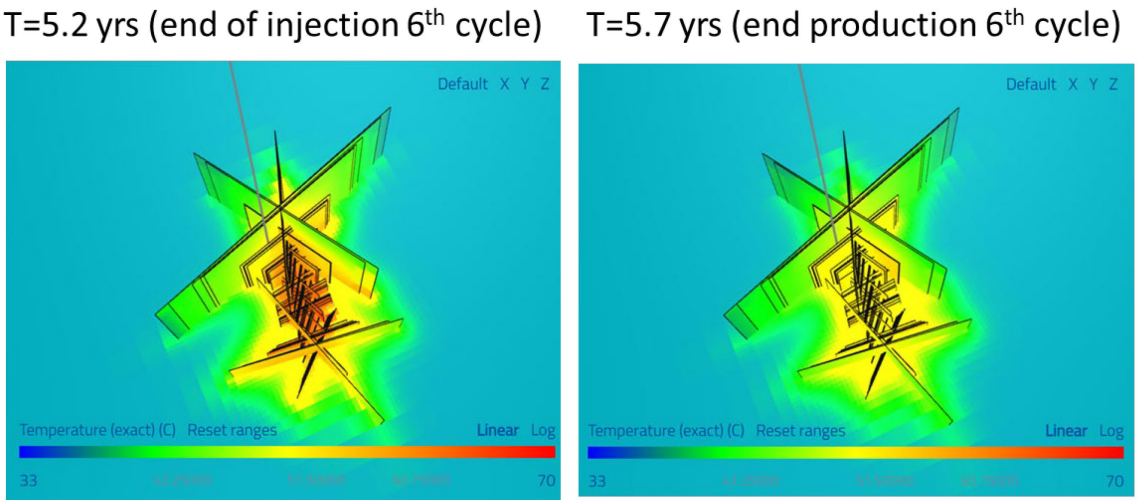


Figure 14: Screenshots of the single well model showing the temperature in the reservoir during injection and production in the last cycle – the 6th year.

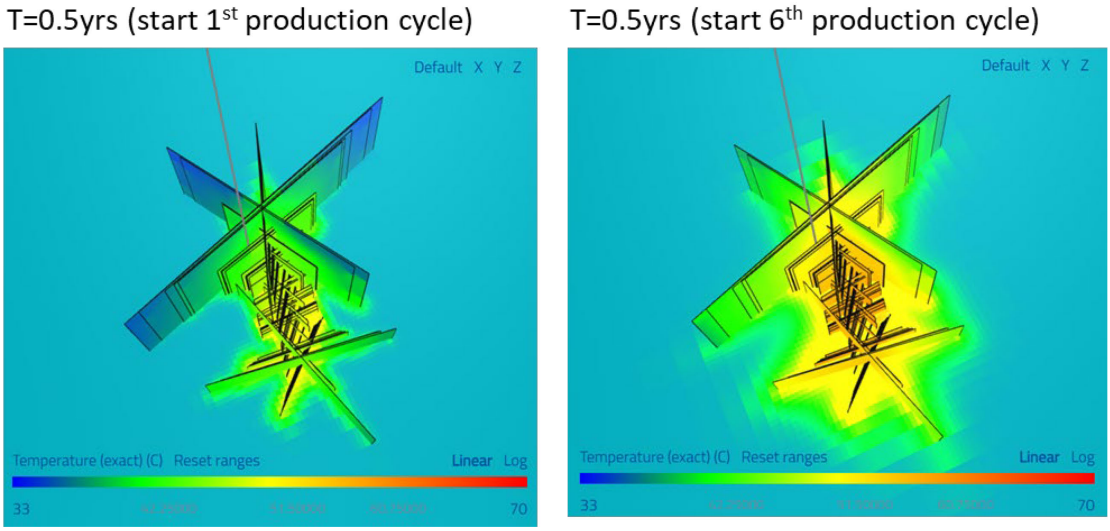


Figure 15: Screenshots of the single well model showing the temperature increasing in the reservoir from Year 1 to Year 6.

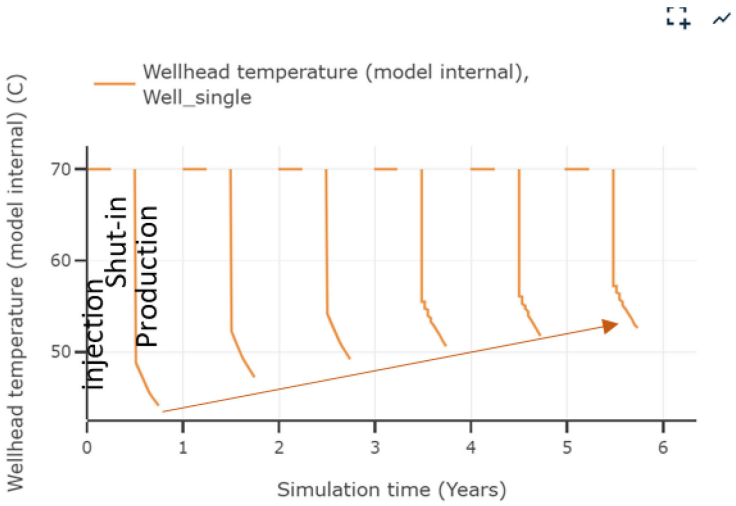


Figure 16: Results from the single well model showing the increase in the production temperature throughout the cycles.

## 3.3 Double well model results

In the two well configuration, Well 1 injects for 3 months in the summer (70˚C) and produces for 3 months in the winter, and Well 2 does the opposite – producing for 3 months in the summer (i.e. to balance the injected water) and injecting a 20°C water for 3 months in the winter. This conceptionally mimics the outlet water from surface heat exchanger that uses the heat of the produced water to bring a water circulation system (e.g., a district heating system) to the desired level. Effectively, Well 1 is storing waste heat from the summer months, while Well 2 is storing cool temperatures from the winter months.

Injection and production are performed at a rate of 0.02 $m^3/s$. Note that the single well model is permitted to inject and produce at a higher maximum rate (ca. 0.03 - 0.04 m^3/s), because it is operated at constant pressure. As a result, the double well model produces less energy than the single well model in these simulations. This is not necessarily an inherent attribute of double well

models – if the maximum rate had been permitted to be higher, it could have produced similar or greater energy than the double well model. On the other hand, higher rate may have led to greater thermal breakthrough, degrading the performance of the system. In a real system, circulation rate would need to be carefully optimized, considering the number of fracture connections between the wells and the well spacing. This study is solely to assess high-level 'feasibility,' of the designs, and so we do not address these detailed practical optimization questions.

Typically, BHP at reservoir level ranges from around 11.5 to 11.8 MPa during injection and 8.9 to 9.3 MPa during production. As with the single-well case, it is necessary to use a pump to produce at BHP less than the in-situ reservoir pressure in order to maintain balanced production and injection.

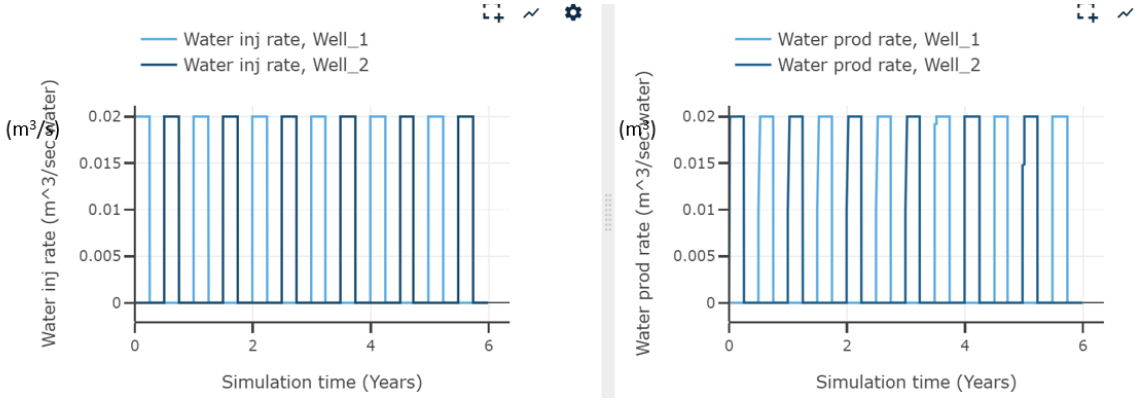


Figure 17: Results from the double well model showing the injection and production rates for Well 1 and Well 2.

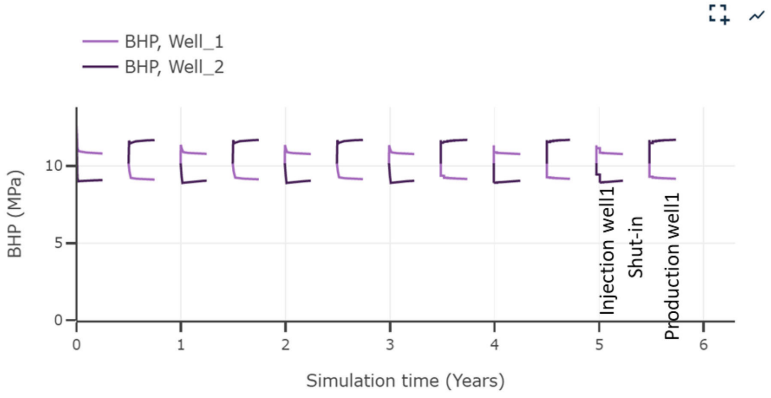


Figure 18: Results from the double well model showing the bottomhole pressure for Well 1 and Well 2.

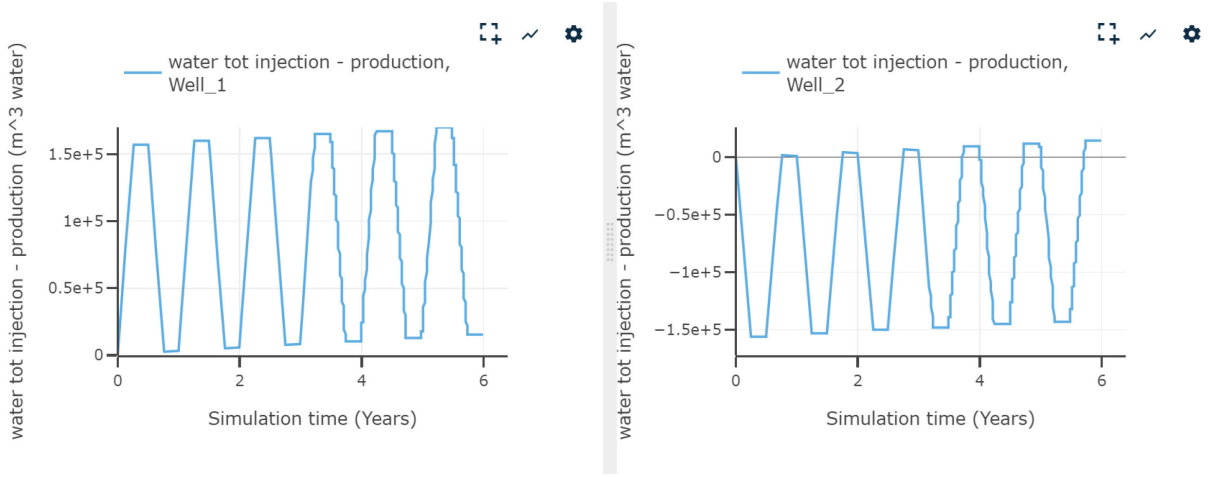


Figure 19: Results from the double well model showing the cumulative volume injected minus the cumulative volume produced for Well 1 and Well 2.

The simulation results show that during the production periods, both wells produce in the range of around 38-45˚C. Well 1, which injects hot water, tends to start at a relatively high production temperature, which then declines over time. Well 2, which injects cold water, observes the opposite trend – relatively low production temperature, which then increases over time. Fluid from the injecting well tends to break through towards the producing well, and so the temporal trend shows a tendency to transition towards the temperature of the injection fluid.

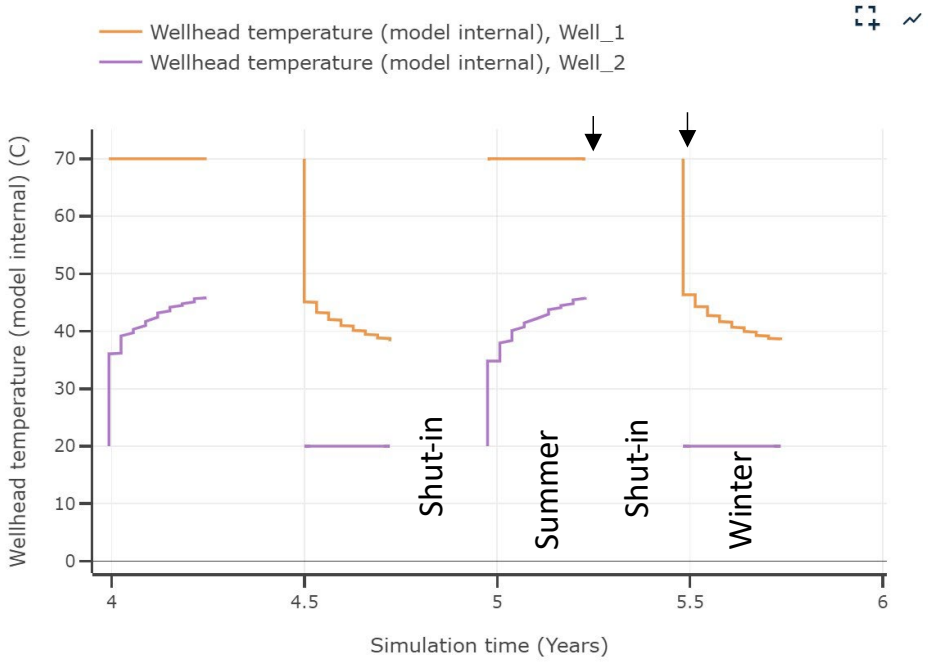


Figure 20: Results from the double well model showing the injection and production temperature during the final year.

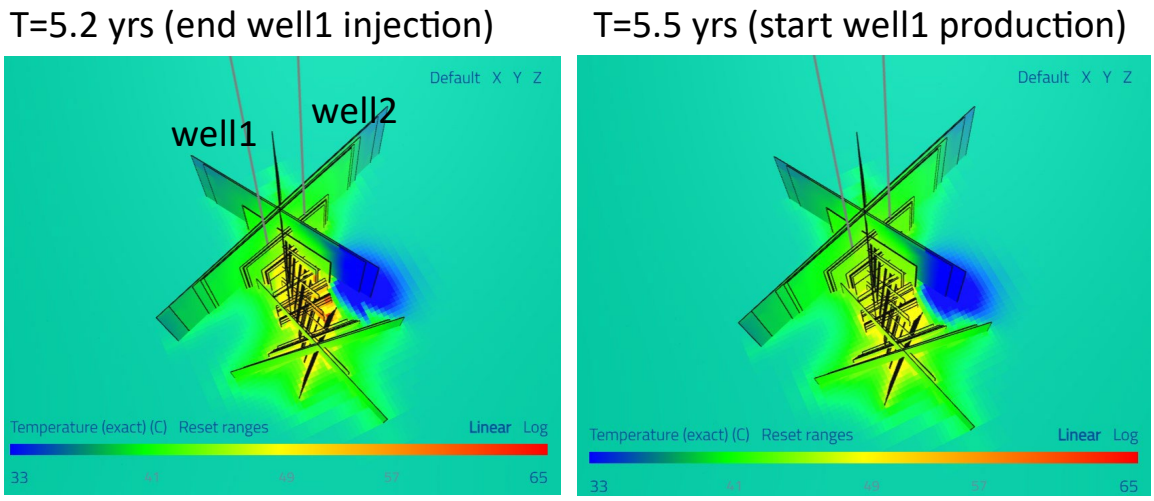


Figure 21: Screenshot from the double well model showing the temperature in the reservoir at two points in time.

## 3.4 Power input/output and energy storage

To calculate the thermal energy ‘input’ and ‘output’ from the system, we consider temperature changes relative to a ‘baseline’ temperature. We tested using either 20˚C or 34˚C.

**Energy input calculation:**

$$Energy\ input\ (kW-hr) = \frac{(Temp_{injection} - 20°C) * (Heat\ capacity\ water)\left(\frac{kJ}{kg-C}\right) * (Injection\ rate)\left(\frac{m^3}{s}\right) * (Density\ water)\left(\frac{kg}{m^3}\right) * Duration(sec)}{3600}$$

**Energy output calculation:**

$$Energy\ output\ (kW-hr) = \frac{(Temp_{production} - 20°C) * (Heat\ capacity\ water)\left(\frac{kJ}{kg-C}\right) * (Injection\ rate)\left(\frac{m^3}{s}\right) * (Density\ water)\left(\frac{kg}{m^3}\right) * Duration(sec)}{3600}$$

## Single well configuration

Figures 22 and 23 below show the cumulative energy input/output from the subsurface over six years for the single well configuration. “Energy stored in the reservoir” (or equivalently, “energy lost in the reservoir”) can be defined as equal to ‘energy input’ minus ‘energy output.’ The energy storage increases during the period of injection and decreases during the periods of production. The production periods produce back less energy than was inputted, resulting in a net increase in energy storage over time (corresponding to inefficiency of the system, which is unable to fully recover the energy inputted to the system).

The calculations assume a baseline temperature of 20˚C. In a conceptual and simplified way, this mimics the scenario that hot injected water was heated by waste heat from a 20°C level and that heat is extracted (e.g. by a heat pump) so that the temperature of the produced water falls to 20°C again.

For the 6$^{th}$ year cycle, the net energy input/output and loss were:

- Thermal energy injected into the reservoir / 1 year cycle= 16.5 GWh
- Thermal energy produced from the reservoir / 1 year cycle =11.7 GWh
- Net thermal energy lost in the reservoir / 1 year cycle= 4.8 GWh


Figure 22: Results from the single well model showing the energy stored in the reservoir: energy inputted minus produced.

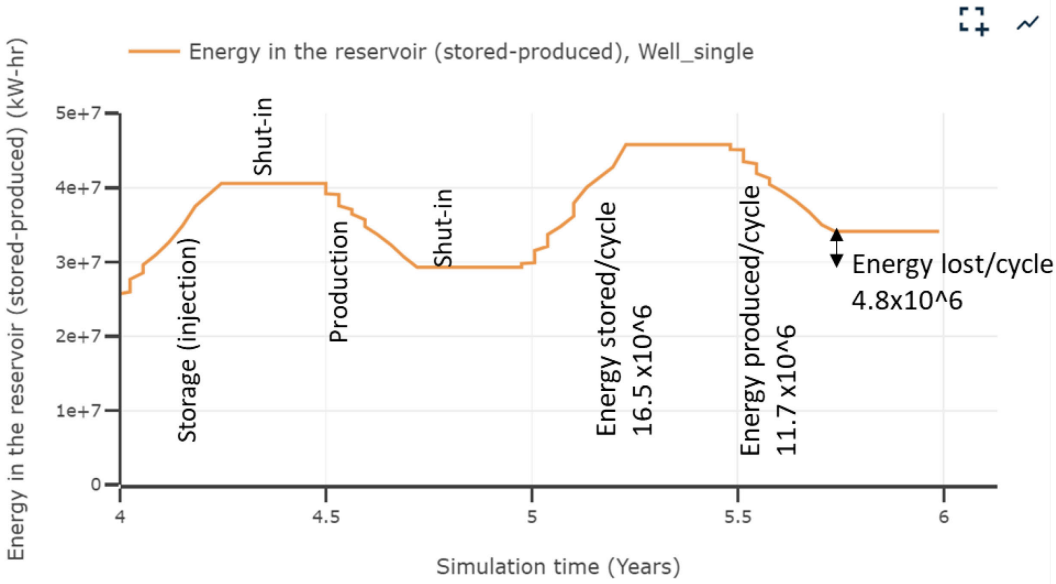


Figure 23: Results from the sixth year of the single well model showing the energy stored in the reservoir: energy inputted minus produced.

Figure 24 shows the thermal power input/output during the injection/production cycles. The average power produced during the 6$^{th}$ production cycle is ~ 5.4 MW.


Figure 24: Results from the single well model showing the power input and output over the six one year cycles.

## Two well configuration

Figures 25 and 26 below show the cumulative energy input/output from the subsurface over six years for the double well configuration. “Energy stored in the reservoir” increases during the period of injection and decreases during the periods of production. The production periods produce back less energy than was inputted, resulting in a net increase in energy storage over time. The calculations assume a baseline temperature of 20˚C.

For the 6$^{th}$ year cycle, the net energy input/output and lost were:

- Thermal energy injected into the reservoir / 1 year cycle= 5.4 GWh
- Thermal energy produced from the reservoir / 1 year cycle =4.0 GWh
- Net thermal energy lost in the reservoir / 1 year cycle= 1.3 GWh

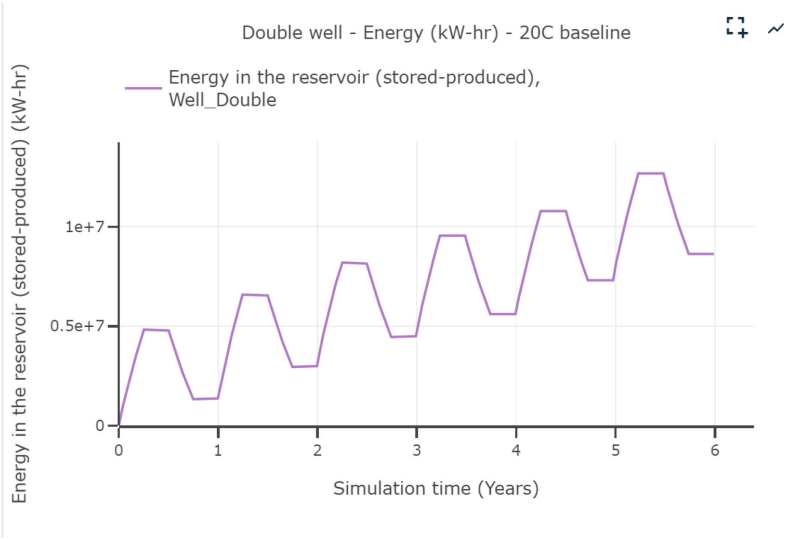


Figure 25: Results from the double well model showing the energy stored in the reservoir throughout the cycles: energy inputted minus produced.

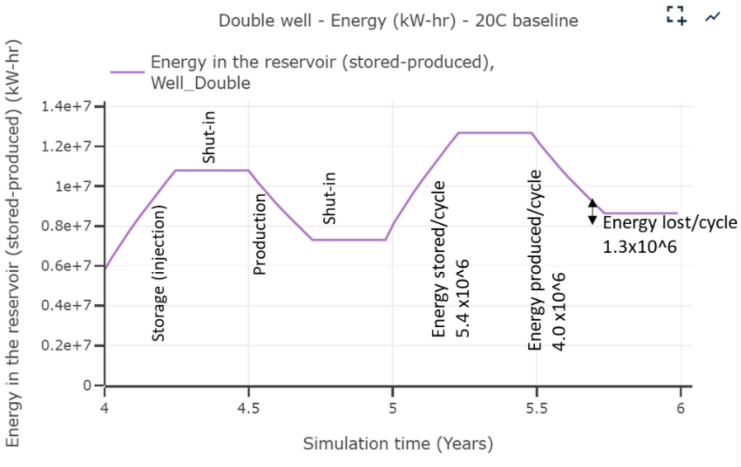


Figure 26: Results from the final year of the double well model showing the energy stored in the reservoir throughout the cycles: energy inputted minus produced.

Figure 27 shows the thermal power input/output during the injection/production cycles. The average power produced during the 6$^{th}$ production cycle is ~ 1,9 MW (range ~ 2.2 to 1.5 MW).

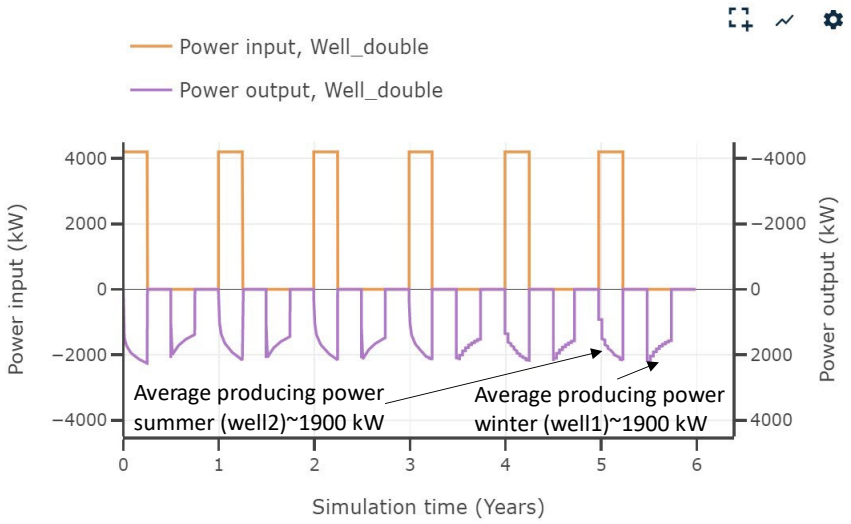


Figure 27: Results from the double well model showing the power inputted and outputted over the six one-year cycles.

## 3.5 Energy efficiency

Cycle efficiency can be calculated as:

$$Energy\ efficiency\ (\%) = \left(\frac{Energy\ produced\ per\ one\ year\ cycle}{Energy\ stored\ per\ one\ year\ cycle}\right) * 100\%$$

The double well model is more efficient than the single well model. The efficiency from the double well model was calculated as 75%, while the efficiency in the single well model was calculated as 71%

| | Single well model | Double well model |
|---|---|---|
| Energy stored 1 year cycle ( kW-hr) | 16,513,000 | 5,367,000 |
| Energy produced 1 year cycle (kW-hr) | 11,683,000 | 4,038,000 |
| Energy lost 1 year cycle (kW-hr) | 4,830,000 | 1,329,000 |
| % Efficiency | 71% | 75% |

## 3.6 Consideration of the power and energy consumed by the suction pump

The use of a suction pump in the well is necessary to increase the flowing bottomhole (BH) pressure during the production cycle, allowing the system to balance injection and production volumes. It was considered important to maintain a balance of water volumes in the reservoir throughout the injection and production cycles.

The power input and energy consumption from the suction pump was considered and calculated using the equation below:

$$Pump\ power\ input\ (kW) = \frac{(Injection\ rate)\left(\frac{m^3}{s}\right) * g\left(\frac{m}{s^2}\right) * (Increase\ in\ hydrostatic\ head)(m) * Density\left(\frac{kg}{m^3}\right)}{1000 * (Efficiency)}$$

The efficiency was assumed to be 80%.

In the single well model, the cumulative total energy consumption from the suction pump is 1.7 million kW-hr in over six years, and the calculated power consumption ~ 140 kW. The suction pump power and energy required are relatively small in comparison to the energy and power from the system.

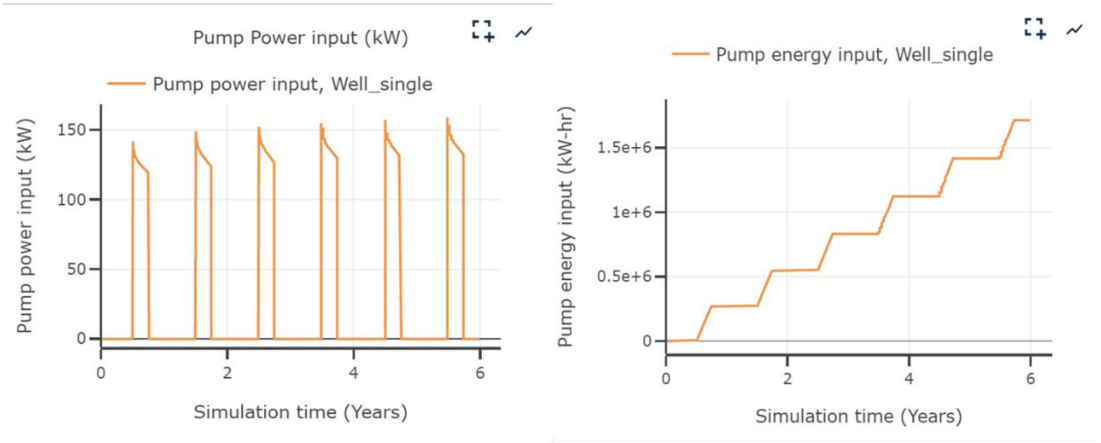


Figure 28: Results from the single well model showing the pump power consumption and cumulative energy consumption versus time.

In the double well model, the cumulative total energy consumption from the suction pump is 0.6 GWh over six years, and the calculated power consumption ~ 20-25 kW. Again, the suction pump power and energy required are relatively small in comparison to the energy and power from the system. The energy and power consumption from the double well model is lower than the consumed power and energy in the single well model because of the pressure support from the injection well.

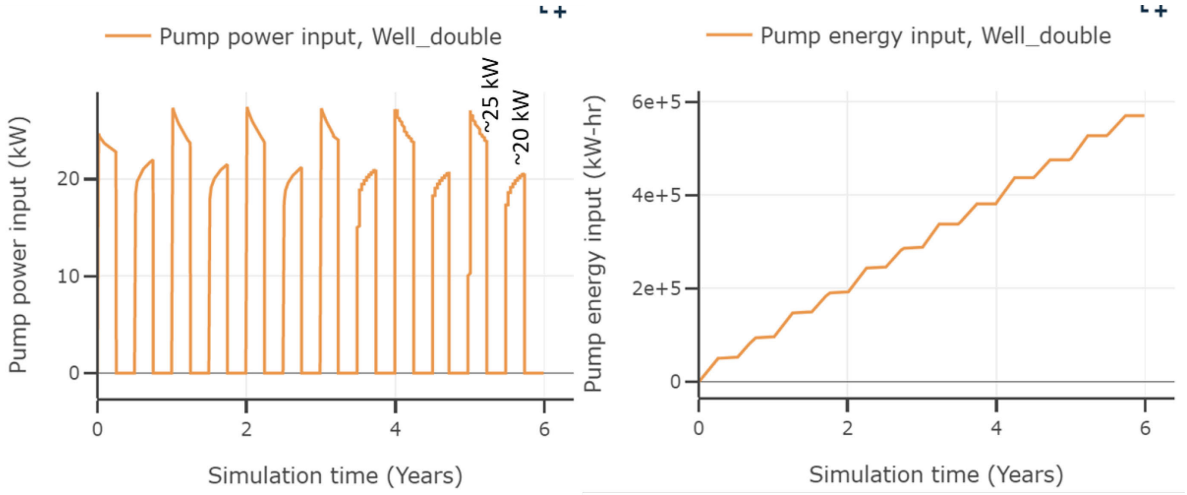


Figure 29: Results from the double well model showing the pump power consumption and cumulative energy consumption versus time.

## 3.7 Sensitivity on well spacing with the double well system

Sensitivity analysis simulations were performed to evaluate the impact of well spacing in the two well configuration. Simulations tested spacings of: 25 m, 50 m, 100 m and 200 m.

The maximum water injection and production rates were specified to be 0.02 $m^3/s$. The results show the maximum water injection and production rates (0.02 $m^3/s$) were achieved with all the different well

spacings between 25 m to 200 m. Figure 30 below shows an example of the injection and production rates achieved on both wells with 100 meter well spacing.

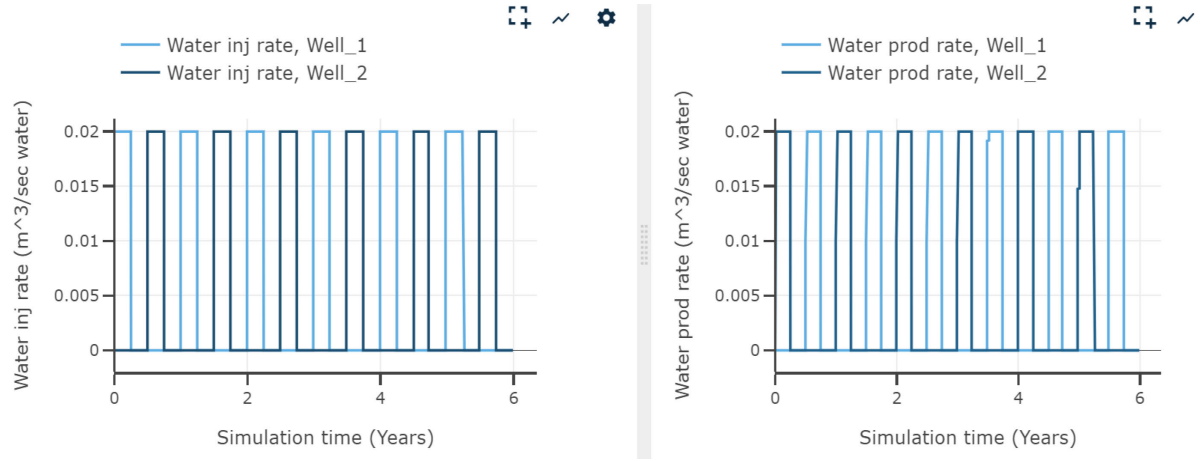


Figure 30: Results from the double well model showing the injection and production rates for Well 1 and Well 2 with 100 m well spacing. The injection and production rates were not different in the simulations with different wells spacings.

The water injection and production volumes do not change with different well spacing; they all reach a good balance water volume in the reservoir at the end of each one-year cycle.

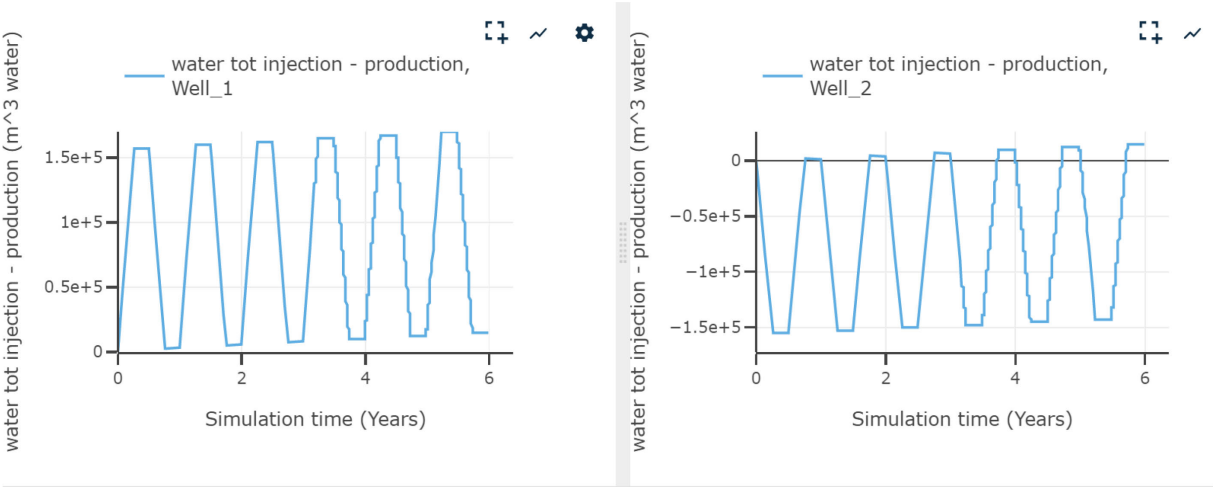


Figure 31: Results from the double well model with 100 m well spacing showing cumulative fluid injected minus cumulative fluid produced.

The produced power increases with well spacing from very low 600 kW (25 m well spacing) to 2600 kW (200 m well spacing). Power production during winter from Well 1 is optimized by increasing well spacing from 50 m to somewhere in the range of 100 to 200 m well spacing.

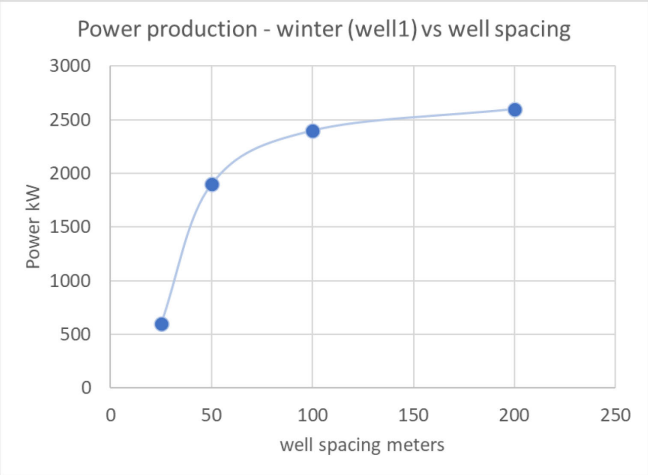


Figure 32: Results from the double well model showing the power production of Well 1 during winter as a function of well spacing.

### Power with model with 25 m well spacing

Figure 33 shows the power input and output for the model with 25 m well spacing. The average power produced during the winter from Well 1 is ~ 600 kW, which is lower than 1,900 kW obtained with 50 m well spacing (base case). Performance is degraded by thermal breakthrough between the injection and production wells.

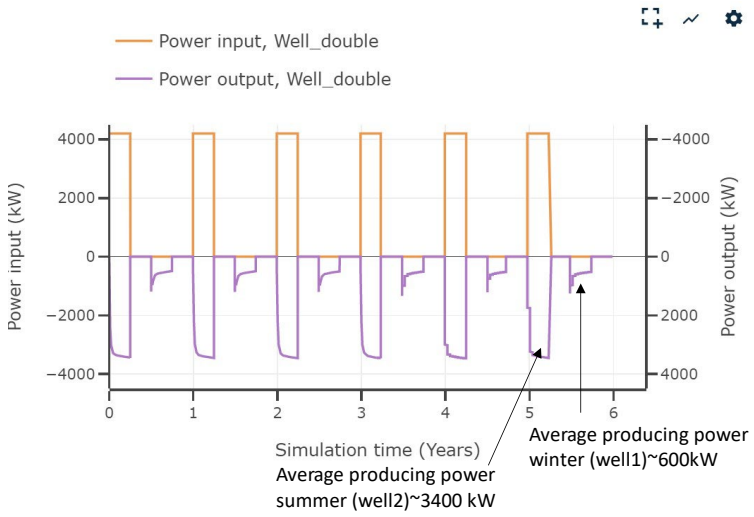


Figure 33: Results with double well model with 25 m well spacing showing power production (output) from Well 1 (winter) and Well 2 (summer).

### Power with model with 50 m well spacing (base case model)

50 m well spacing is the base case model. Its average power produced during the winter from Well 1 is ~ 1900 kW. This is the reference model for the sensitivity of well spacing.

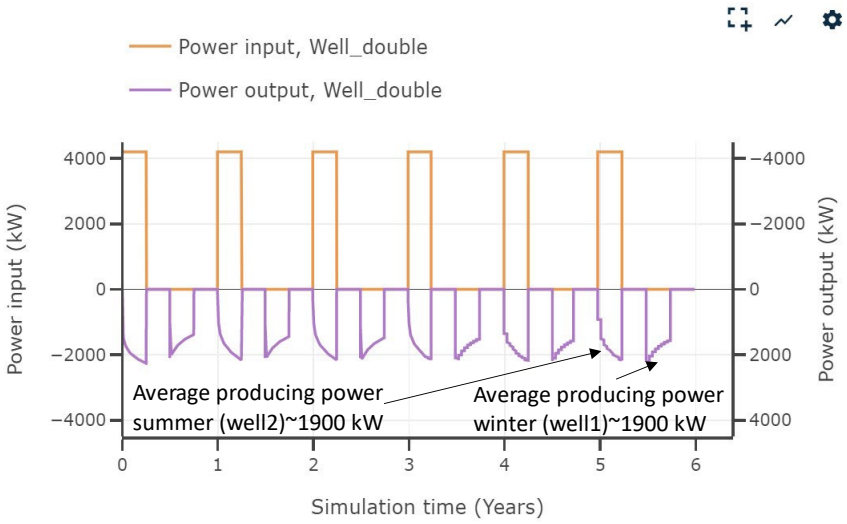


Figure 34: Results with double well model with 50 m well spacing showing power production (output) from Well 1 (winter) and Well 2 (summer).

### Power with model with 100 m well spacing

The average power produced during the winter is ~ 2400 kW, which is higher than 1,900 kW obtained with 50 m well spacing (base case).

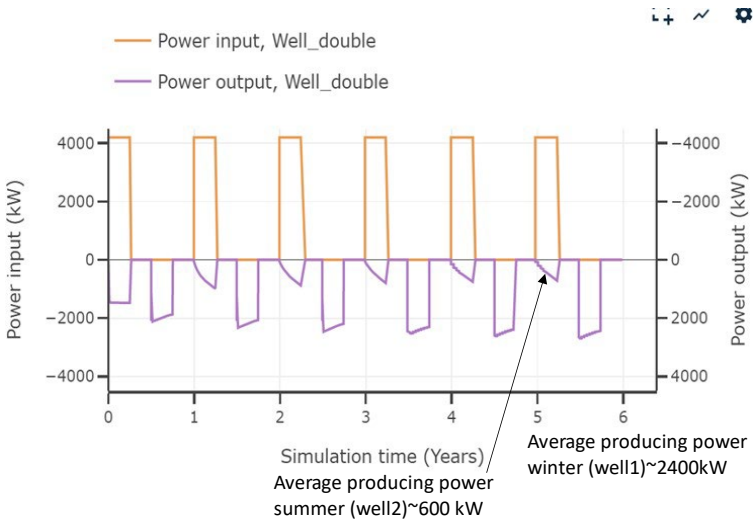


Figure 35: Results with double well model with 100 m well spacing showing power production (output) from Well 1 (winter) and Well 2 (summer).

### Power with model with 200 m well spacing

The average power produced during the winter is ~ 2600 kW, which is higher than 1,900 kW obtained with 50 m well spacing (base case).

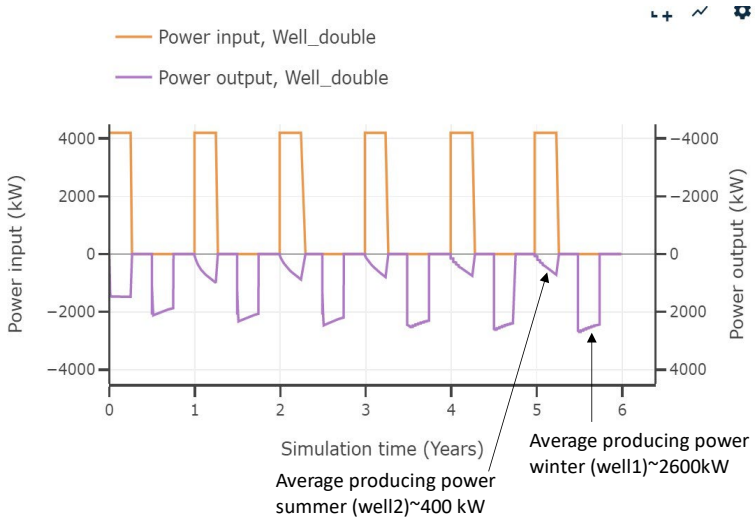


Figure 36: Results with double well model with 200 m well spacing showing power production (output) from Well 1 (winter) and Well 2 (summer).

### Energy with different well spacings

The energy stored and energy produced increase with well spacing. The values of energy stored and produced reaches their maximum with ~100 to 200 m of well spacing.

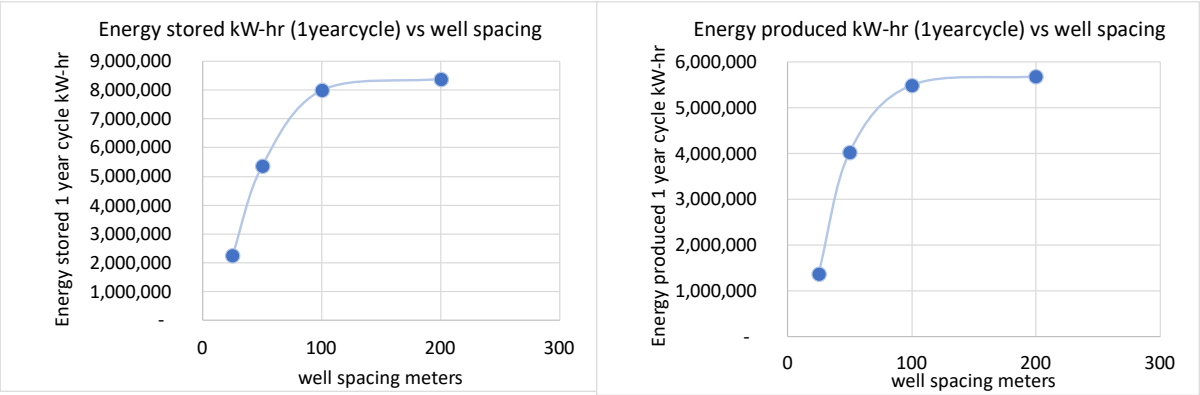


Figure 37: Results with double well model showing energy storage and production per one-year cycle as a function of well spacing.

The energy efficiency was also calculated for all the different well spacings from 25 to 200 m. The result indicates similar efficiencies with wells spacings between 50 to 200 m, showing efficiencies in the range of 68-75% and relatively lower efficiency (61%) for the case with 25 m well spacing.

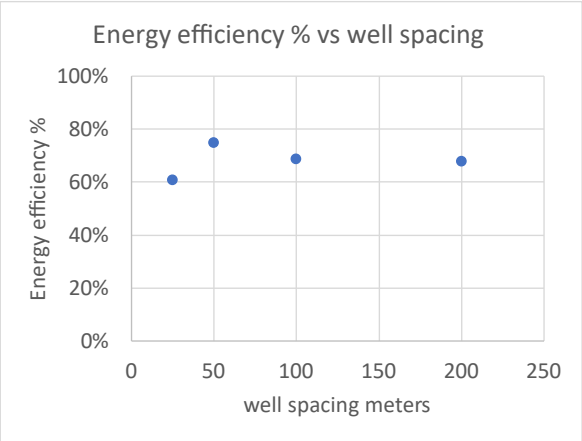


Figure 38: Results with double well model showing storage efficiency as a function of well spacing.

## Energy from model with 25 m well spacing

- Thermal energy injected into the reservoir / 1 year cycle = 2.2 GWh
- Thermal energy produced from the reservoir / 1 year cycle = 1.4 GWh
- Net thermal energy lost in the reservoir / 1 year cycle = 0.9 million GWh
- % efficiency = 61%

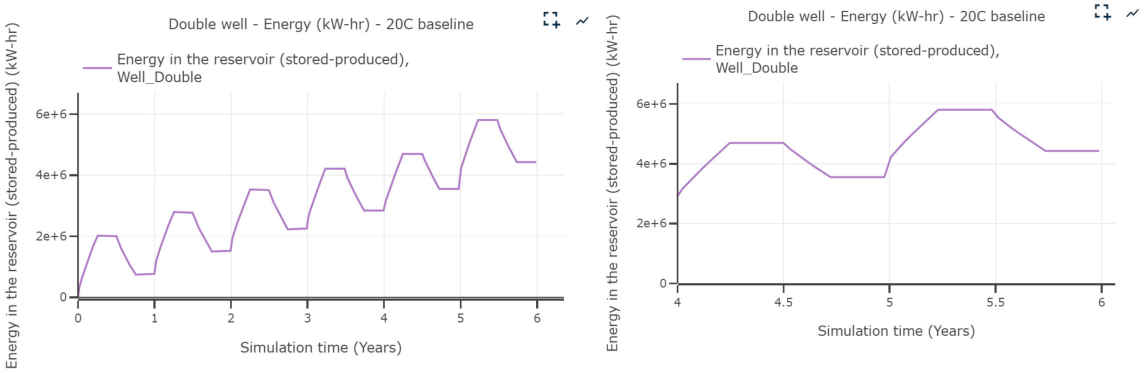


Figure 39: Results from the double well model with 25 m well spacing, showing net energy stored in the reservoir as a function of time.

## Energy from model with 50 m well spacing (base case model)

- Thermal energy injected into the reservoir / 1 year cycle = 5.4 GWh
- Thermal energy produced from the reservoir / 1 year cycle = 4.0 GWh
- Net thermal energy lost in the reservoir / 1 year cycle = 1.3 GWh
- % efficiency = 75%

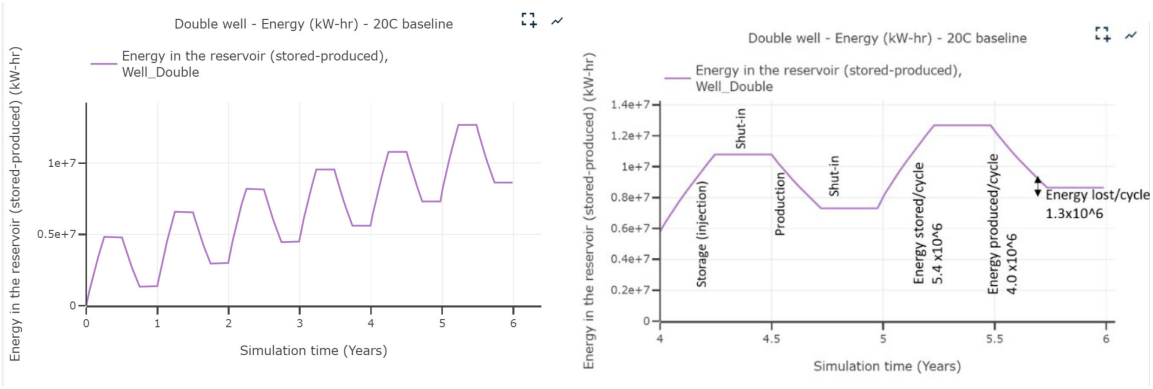


Figure 40: Results from the double well model with 50 m well spacing, showing net energy stored in the reservoir as a function of time.

## Energy from model with 100 m well spacing

- Thermal energy injected into the reservoir / 1 year cycle = 8 GWh
- Thermal energy produced from the reservoir / 1 year cycle = 5.5 GWh
- Net thermal energy lost in the reservoir / 1 year cycle = 2.5 GWh
- % efficiency = 69%

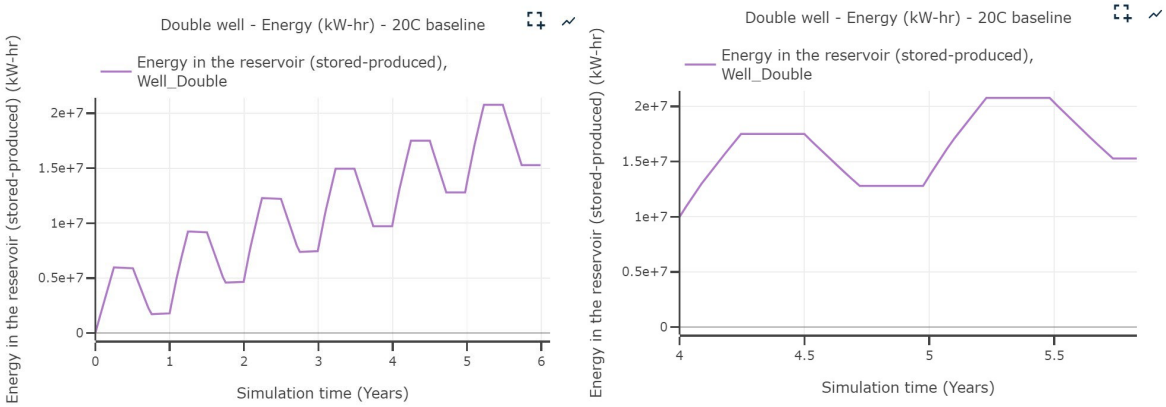


Figure 41: Results from the double well model with 100 m well spacing, showing net energy stored in the reservoir as a function of time.

## Energy from model with 200 m well spacing

- Thermal energy injected into the reservoir / 1 year cycle = 8.4 GWh
- Thermal energy produced from the reservoir / 1 year cycle = 5.7 GWh
- Net thermal energy lost in the reservoir / 1 year cycle = 2.7 GWh
- % efficiency = 68%

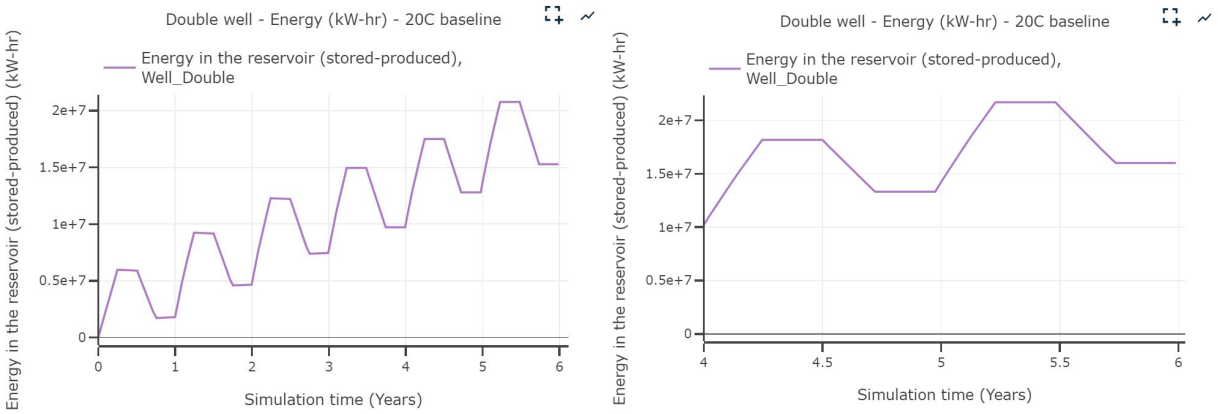


Figure 42: Results from the double well model with 200 m well spacing, showing net energy stored in the reservoir as a function of time.

# 4 Conclusions

The modeling results suggest that thermal energy storage through seasonal injection/production is feasible in fractured crystalline rock. Both the one and two well configurations were able to achieve good performance, considering both power and thermal efficiency.

In practice, the formation injectivity/productivity will be a critical determining factor for performance. If the system permeability is too low, it will not be possible to achieve sufficient injection and production rates. However, considering parameters inspired by the Bedretto Underground Laboratory, it appears that such injectivities can be achievable, as long as wells utilize extended openhole sections. Borehole orientation can be optimized to maximize the number of natural fractures that are intersected, considering the dominant fracture network orientations. Hydraulic stimulation may be a useful tool to increase injectivity/productivity in the near-wellbore region.

In this study, the formation was sufficiently permeable that the single well configuration was able to achieve good performance. However, in formations with lower permeability, the two well configuration may be more advantageous because it uses injection to balance production, and so mitigates pressure drawdown. This could help maintain sufficient flow rate.

If using a two well configuration, the simulations suggest that well spacing is important to optimize; if the wells are too close-together relative to the circulation rate, system performance can be significantly degraded.

# 5 Outlook and next steps

The next step would be to perform more specific design and analysis of a proposed system for a particular location. Also, technoeconomic analysis is needed to evaluate the levelized cost of the system, to evaluate economic feasibility.

# 6 National and international cooperation

This study was performed in collaboration between a US-based simulation company, ResFrac Corporation, and personnel from the Swiss Federal Office for Energy.

# 7 References


Barnes, Frank S., and Jonah G. Levine. 2011. Large Energy Systems Handbook. CRC Press.

Birdsell, Daniel et al. 2021. Minimum transmissivity and optimal well spacing and flow rate for high-temperature aquifer thermal storage. Applied Energy **289**, 116658.

Bröker, Kai. 2019. In-situ stress and rock mass characterization via mini-frac tests at the Bedretto Underground Laboratory. MS Thesis. ETH Zurich.

Bröker, Kai, and Xiaodong Ma. 2022. Estimating the Least Principal Stress in a Granitic Rock Mass: Systematic MiniFrac Tests and Elaborated Pressure Transient Analysis. Rock Mechanics and Rock Engineering **55**, 1931-1954.

Cabeza, L. 2015. Advances in Thermal Energy Storage Systems: Methods and Applications. Woodhead Publishing Series in Energy: Number 66. Elsevier.

Cho, Won Jin et al. 2010. Thermal properties of granite from KAERI underground research tunnel (KURT). Technical report prepared for the Korea Atomic Energy Research Institute, Daejeon.

David, Christian et al. 2020. On petrophysical and geomechanical properties of Bedretto Granite. ETH Zurich Report.

Giardini, Domenico et al. 2022. Validation of technologies for reservoir engineering (VALTER). Swiss Federal Office of Energy internal report. Publisher: ETH, Geo-Energie Suisse.

Gischig, Valentin S. et al. 2020. Hydraulic stimulation and fluid circulation experiments in underground laboratories: Stepping up the scale towards engineered geothermal systems. Geomechanics for Energy and the Environment **24**.

Göran, Hellström, and Sven Åke Larson. 2001. Seasonal thermal energy storage – the HYDROCK concept. Bulletin of Engineering Geology and the Environment **60**, 145-156.

Janiszewski, Mateusz. 2019. Techno-economic aspects of seasonal underground storage of solar thermal energy in hard crystalline rocks. Doctoral Dissertation. University of Helsinki.

Kushnir, Alexandra et al. 2018. Characterizing the physical properties of rocks from the Paleozoic to PermoTriassic transition in the Upper Rhine Graben. Geothermal Energy **6**.

Ma, Xiaodong et al. 2021. Multi-disciplinary characterizations of the Bedretto Lab – a new underground geoscience research facility. Journal of Geophysical Research: Solid Earth **13**, 301–322.

McClure, Mark. 2017. An accurate and efficient method for calculating fluid exchange between fractures and matrix with a non-confirming mesh. arXiv:1709.02493.

McClure, Mark, Charles Kang, Chris Hewson, Soma Medam, Egor Dontsov, and Ankush Singh. 2022. ResFrac Technical Writeup. 12th Edition. arXiv:1804.02092.

Nordell, Bo, and Göran Hellström. 2000. High temperature solar heated seasonal storage system for low temperature heating of buildings. Solar Energy, **69**(6), 511–523.

Pavlov, Georgi, and B.W. Olsen. 2012. Thermal energy storage - A review of concepts and systems for heating and cooling applications in buildings: Part 1 – Seasonal storage in the ground. HVAC&R Research **18**(3), 515-538.

Ricks, Wilson, Jack Norbeck, and Jesse Jenkins. 2022. The value of in-reservoir energy storage for flexible dispatch of geothermal power. Applied Energy **313**.